Rakenteiden Mekaniikka (Journal of Structural Mechanics)
Vol. 58, No. 2, 2025, pp. 71–85
https://rakenteidenmekaniikka.journal.fi/index
https://doi.org/10.23998/rm.152481

Computer vision framework for crack detection and estimation of air leakage through the straight-through cracks in buildings envelopes

Maliheh Jahanbakhsh[1] and Andrea Ferrantelli

Summary Over time, buildings inevitably experience physical and functional deterioration. Regular and accurate inspections are essential to ensure safety and functionality, helping to avoid hazardous and uncomfortable conditions. Cracks, a common indicator of structural distress, also facilitate air infiltration due to pressure differences between the interior and exterior. The precise and efficient detection of cracks, along with the estimation of air infiltration through these cracks, is therefore critical for civil engineering applications that aim to reduce energy consumption and enhance indoor air quality. This paper introduces a novel image processing framework for automatic detection of cracks in building envelopes, coupled with the measurement of indoor and outdoor air parameters, which could be used to assess crack size and to estimate air infiltration rates by using heat transfer and fluid mechanics formulas. A computer vision-based system for automatic crack detection is first developed by using the Python OpenCV library through binarization, Otsu's thresholding and Canny operator; geometric quantification of the cracks is then obtained via skeletonization, and the resulting morphological characteristics of the cracks are finally used to estimate airflow by using common fluid mechanics formulas.

Keywords: crack detection, computer vision-based methods, crack geometry, airflow

Received: 29 November 2024. Accepted: 3 June 2025. Published online: 23 June 2025.

Introduction

Building infiltration has been identified as a critical factor influencing the thermal load of structures. The extent of this impact varies depending on climatic conditions and building specific factors, such as construction type and design. According to the revised Finnish Building Code [1], the average infiltration rate is determined by dividing the air leakage rate, n_{50}, measured during a single pressurization test, by 25. Here, n_{50} represents the air change rate per hour under a pressure differential of 50 Pa. This standardized approach provides a benchmark for assessment building infiltration and its contribution to energy performance metrics [2].

The thermal load associated with entering outdoor air into a building's interior is conventionally understood to be predominantly influenced by the infiltration flow rate and the temperature differential between indoor and outdoor environments [3]. In tall

[1]Corresponding author: maliheh.jahanbakhsh@aalto.fi

buildings, the stack effect serves as the primary mechanism driving air infiltration. This phenomenon arises due to variations in air buoyancy caused by differences in temperature across the building envelope, compounded by the building's vertical height, which collectively establish a pressure differential between the internal and external environments [4]. Research indicates that air infiltration contributes substantially to the overall heating demand, accounting for 25% to 50% of the heating load in residential and commercial structures, and approximately 15% of heating loads in commercial buildings can be attributed to air infiltration [5]. Furthermore, there is evidence that also harmful chemical and microbiological agents from outdoors and even from the structures themselves can leak into the living spaces and affect the indoor air quality of the occupants (see e.g. [6] and references quoted therein).

A study investigating air infiltration through cracks in timber floors revealed that infiltration is primarily influenced by the size and spatial distribution of cracks, the ventilation of the subfloor, and the pressure differentials across the floor. This emphasizes the necessity of addressing such cracks and implementing improved insulation or sealing measures to optimize energy performance and minimize heating demands [7].

Minimum outdoor air ventilation rates, as outlined e.g. in ASHRAE Standards [3], are typically determined based on parameters including the air tightness of the building envelope, total floor area, geographical location, and number of occupants. Such Standards incorporate a constant infiltration credit, which allows for a reduction in the mechanical ventilation requirement. However, actual infiltration rates are influenced by dynamic factors such as weather conditions and system operation. Consequently, if real-time infiltration rates were available and utilized to adjust mechanical ventilation rates, mechanical systems could potentially operate more efficiently. Theoretical controllers designed to dynamically adjust the hourly mechanical ventilation rate to satisfy ventilation requirements could result in substantial annual average energy savings, as shown in [8].

Despite its significance, air leakage through cracks as a factor in infiltration calculations has not been adequately explored regarding its potential impact.

Previous studies have primarily focused on crack detection and segmentation using image processing techniques, as well as analyzing airflow through various types of cracks via experimental methods or simulations. In this study, the airflow through the crack is examined with respect to the impact of pressure differentials on building envelopes, which are caused by the height of the envelope above ground level. This is achieved through airflow estimation by using physical formulas, considering the correlation between the geometrical parameters of the crack surface and the airflow passing through, without relying on experimental or simulation approaches to enhance applicability for automation.

Integrating morphological studies of cracks with their implications for infiltration and building thermal loads is essential for accurately estimating the energy demands of buildings in a rapid or real-time manner. To achieve this, the development of an automated framework for the detection and characterization of crack geometry is imperative. Such a framework would enable real-time estimation of airflow through cracks, facilitating precise calculation of thermal loads and supporting enhanced energy efficiency strategies.

This study presents the development of an integrated framework aimed to automate the detection and morphological characterization of cracks using advanced computer vision techniques. The framework incorporates a computational script to estimate airflow through cracks, accounting for the stack effect, thereby streamlining and automating the analysis process. To demonstrate the practical application and robustness of the framework, a representative case study has been conducted, illustrating its effectiveness in real-world scenarios.

For the estimation of airflow, the framework leverages existing research that models airflow through cracks and includes physical studies on this phenomenon. In these studies, the pressure flow characteristics of various full scale model cracks, representative of real-world leakage paths, have been systematically measured. These measurements validate the crack flow equations across a vast range of parameters.

The model uses a quadratic relationship for the pressure drop ΔP characteristics,

$$\Delta P = A \cdot Q + B \cdot Q^2 \,, \tag{1}$$

which serves as an alternative to the commonly employed power-law approximation for pressurization data. In Eq.(1), the quadratic coefficients A and B are directly tied to the physical parameters of the crack, providing a more practical and physically grounded approach. Furthermore, a simple graphical method is introduced to facilitate the prediction of crack leakage areas based on these coefficients [9, 10].

Using this theory, the framework can estimate airflow through three types of cracks: straight-through cracks, L-shaped cracks, and Double-bend cracks. This capability enhances the applicability of the framework for diverse building conditions and supports accurate and automated predictions of thermal and energy performance [9].

Methodology

This research introduces a novel image-based methodology for estimating airflow through structural cracks. The proposed framework, delineated in figure 1, encompasses a systematic approach comprising three principal stages aimed at automating crack detection and quantifying their geometric parameters, including width and length. These metrics are subsequently utilized to infer airflow through the cracks, enabling precise air infiltration calculations for building envelopes under a hypothetical worst-case scenario.

This scenario assumes that the identified cracks traverse the entire wall thickness, facilitating unrestricted airflow to the exterior. The initial stage involves advanced crack detection techniques leveraging image processing algorithms that are applied to high-resolution photographs of wall surfaces exhibiting cracks. This stage ascertains the presence and location of cracks with high reliability. The subsequent stage encompasses the precise quantification of crack dimensions, including the determination of maximum, minimum, and mean widths, as well as the estimation of crack length based on image data. These measurements are integrated into the final stage, where they are employed to compute air leakage due to the stack effect, which is a key parameter for assessment the structural and energy performance of the building envelope.

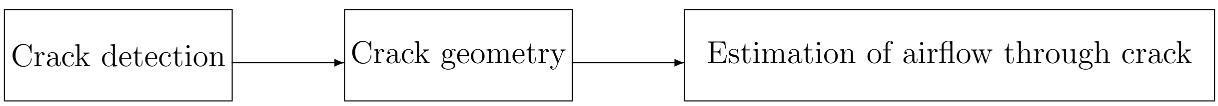

Figure 1. Framework of the crack detection, inference of geometry and through-crack airflow estimation

Detection and geometric characterization of cracks

The first two steps of the methodology propose a framework for automation of crack detection and geometric quantification, as portrayed in the flowchart in figure 2. The first step is an *autonomous detection of the crack through camera pictures* involving image processing, which articulates as follows:

(1) gathering the images of the surface by camera,
(2) pre-processing the collected pictures with image processing to remove noise,
(3) thresholding with segmentation to distinguish target object from background,
(4) applying the Canny operator to visually distinguish the crack, leading to detection.

The second step is *crack feature extraction*, where the detected cracks are separated based on the width, depth and direction of propagation of the crack. In this study, Python's OpenCV library is utilized as a robust and versatile tool for image processing, enabling efficient implementation of algorithms for tasks such as noise reduction, grayscale conversion, edge detection, and feature extraction.

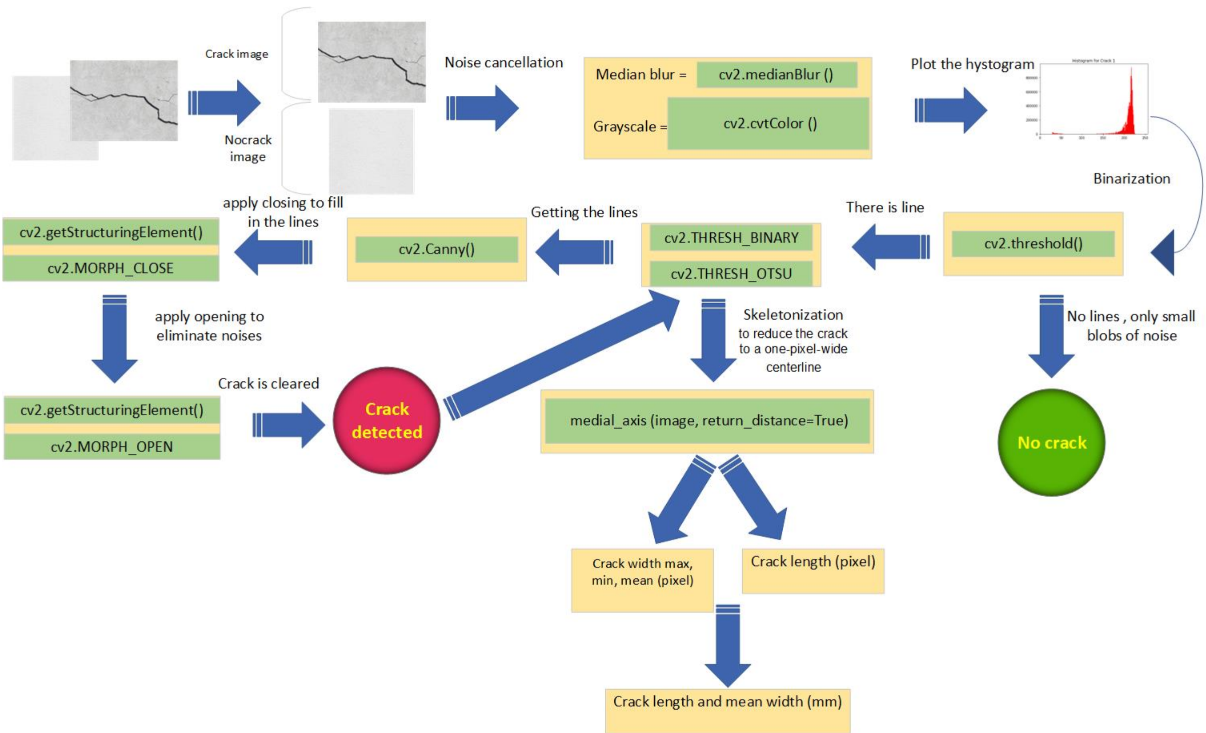

Figure 2. Crack detection and geometric quantification

In summary, the algorithm proposed in figure 2 first processes an input image to filter noise and detect cracks by means of a connected component analysis, then connected regions in the binary image are identified. After conducting filtering based on a minimum size threshold, the algorithm then checks if cracks are present by analyzing the number of unique connected components. In the output, crack presence or good wall condition will be indicated with a message and visualization.

Crack detection

In the domain of image pre-processing, two fundamental steps are involved: (1) noise reduction using a median filter, and (2) conversion to grayscale. During real-time image acquisition, crack images often encounter various challenges, such as shadows, inadequate illumination, raindrops, superficial scratches, and other surface irregularities. These factors can significantly elevate the rate of false-positive detections in subsequent analysis.

Consequently, noise reduction is a critical pre-processing step within any image-based crack detection framework. Enhanced image datasets can be obtained through a range of pre-processing techniques, including contrast enhancement, shadow mitigation, and cropping unnecessary regions.

The primary challenge in crack detection is the pervasive presence of noise, which complicates the accurate identification of pixels associated with cracks. Several pre-processing methods, including filtering and smoothing, are routinely applied to enhance image quality and ensure accurate crack identification. Among these, filtering techniques, such as median blurring, are commonly employed to smooth images and remove noise, while simultaneously preserving important edge information [11–14].

The median filter, in particular, is utilized to attenuate both noise and shadow artifacts in the image [15]. As a non-linear filter, it is particularly effective in reducing noise while preserving essential structural details, especially edges. Let the input image be denoted by $I(x, y)$, with the median filter operating via a sliding window (or kernel) of size $m \times n$ centered on each pixel (x, y). The output pixel value $I_{\text{med}}(x, y)$ at each location is computed as the median value of the pixels within the window:

$$I_{\text{med}}(x, y) = \text{Median}\left\{I(u, v) \mid (u, v) \in \mathcal{N}(x, y)\right\} . \tag{2}$$

In this formulation, $\mathcal{N}(x, y)$ in Eq.(2) represents the set of pixels in the neighborhood of pixel (x, y), typically defined by a square region of size $m \times n$ around the pixel. The median operator Median$(\cdot)$ selects the middle value from the sorted list of pixel intensities within this neighborhood [16]. This approach makes the median filter highly effective in mitigating impulse noise, such as salt-and-pepper noise, while maintaining the sharpness of edges in the image. The median blur in figure 2 has 2 parameters, namely image and kernel size. The kernel size must be odd, e.g. 3, 5, 7. The larger kernels cause stronger smoothing, but risk removing thin cracks [17]. For this reason, in the present case the kernel size is set to 5.

After mitigating noise through median blurring, grayscale conversion enhances the discernibility of cracks in the images and simplifies the image analysis process by reducing the dimensionality of the data, since an RGB image that encompasses three color channels (red, green, and blue), is transformed into a single-channel brightness scale. This reduction compresses the data volume by approximately two-thirds, significantly decreasing computational complexity and expediting both algorithm training and crack identification. The conversion process is underpinned by the luminous efficiency of the constituent color channels. Due to the varying sensitivity of the human visual system to different wavelengths, green is perceived as the brightest color, while blue appears as the darkest [16]. The most common grayscale conversion methods are average, luma, and luminance [18]. The International Commission on Illumination (CIE) has established standardized weights for computing the true luminance (Y) of a pixel on modern displays, based on the linear contributions of red (R), green (G), and blue (B) channels. The luminance calculation is expressed mathematically as in Eq.(3):

$$Y = 02125R + 0.7154G + 0.0721B = 0 . \tag{3}$$

Thresholding is a widely used technique in image processing for crack detection [19]. It involves converting a grayscale image, where pixel intensity values range from 0 (black) to 255 (white), into a binary image. In this process, each pixel's intensity is compared to a predefined threshold value: pixels with intensity below the threshold are assigned a black (0) value, while those above the threshold are assigned a white (255) value [20]. Otsu's method, a popular thresholding approach, is extensively employed in various image processing applications [21]. This method assumes that an image can be segmented into two distinct groups: the background and the target object. The threshold value is determined by maximizing the between-class variance, which quantifies the separation between these two groups. This variance serves as a measure of homogeneity in the pixel intensity distribution, enabling the automatic selection of an optimal threshold for effective segmentation. Otsu's algorithm searches for the threshold t that minimizes intra-class variance. Their formulations are expressed as shown in Eq.(4),

$$\sigma_w^2(t) = q_1(t)\sigma_1^2(t) + q_2(t)\sigma_2^2(t)\,, \tag{4}$$

where q_1, q_2 represent the probabilities of each class, and σ^2 denotes the variance. In this study, for image thresholding, the maximum intensity value of 255 is assigned to pixels exceeding the threshold. Additionally, at this stage, two Otsu algorithms are applied to automatically determine the optimal threshold and perform binary thresholding. Consequently, pixels with intensities greater than the threshold are set to 255 (white), while pixels with intensities less than or equal to t are set to 0 (black). In other words, thresholding is performed using the computed optimal threshold t, where pixels with values greater than t are assigned the value 255, and those less than or equal to t are given the value 0.

In the next stage, implementation of an edge detector to preserve crack geometry and facilitate efficient analysis is initiated. Generally, edge detectors are mathematical techniques designed to identify points of high gray-level intensity variation within an image [22]. These intensity variations often occur at locations where the gray-level intensity fluctuates dramatically, forming structures known as *edges*. Since fracture pixels are strongly correlated with pixel locations exhibiting abrupt changes in gray-level intensity, edge detection methods are highly effective for identifying cracks in concrete surfaces. Edge-based approaches for fracture detection are thus widely adopted. The *Canny edge operator* is employed for signal enhancement, utilizing two sets of 2×2 matrices: the horizontal and vertical filters. The horizontal and vertical approximation differences in grayscale intensity are computed by performing convolution operations. Let G'_a and G'_b represent the horizontal and vertical edge detection results of the image's gray value, respectively. The Canny operator returns a value for the first derivative in both horizontal and vertical directions. Their formulations are expressed as in Eq.(5) [23]:

$$G'_a = \begin{bmatrix} -1 & 1 \\ -1 & 1 \end{bmatrix} * G\,, \qquad G'_b = \begin{bmatrix} 1 & 1 \\ -1 & -1 \end{bmatrix} * G. \tag{5}$$

After applying the Canny operator, cracks become visually distinguishable in the images, with enhanced contrast between crack pixels and their surroundings.

To further refine the binary image, morphological operations are then employed to extract and analyze image components that are useful for representing and describing shapes, such as erosion, dilation, opening, and closing operations [24]. In this study, a rectangular structuring element (a small kernel matrix) was utilized to perform a combination of morphological operations, including opening and closing, to effectively remove small noise while preserving the primary shapes of the cracks. Opening operations smooth object contours, break narrow isthmuses, and eliminate thin protrusions. In contrast, closing operations also smooth contours but are specifically effective at fusing narrow breaks, filling small gaps, and eliminating small holes within the structure [25]. To achieve the desired refinement, a morphological filter comprising a closing operation followed by an opening operation was applied. This sequence ensures both noise reduction and the preservation of the crack's geometric integrity, facilitating accurate representation and analysis. The morphological opening and closing operations both utilize a kernel parameter. For opening, the kernel has a rectangular shape, and its size should approximate the expected crack thickness. For closing, smaller kernels help eliminate minor speckles while preserving true crack lines. The kernel size for closing is typically 3×3, 5×5 or 7×7, smaller sizes are recommended for thin cracks, while larger sizes are suitable for wider or fragmented cracks. For opening, the kernel size range is the same as for closing, but using excessively large kernels may remove fine cracks. Visual testing is necessary to determine the optimal size [26].

Crack segmentation and geometry quantification

To measure the width and length of a crack after applying Otsu's thresholding, skeletonization can be utilized. Skeletonization involves reducing a binary shape to its center line representation while preserving its structural properties. This process calculates the skeleton by filling the enclosed area of the boundary with foreground pixels and treating it as a binary region. In simpler terms, the skeleton is derived using the coordinates of all points within the region, including those along its boundary.

The concept involves simplifying a region into a graph-based representation by extracting its skeleton, which represents the set of points within a region that are equidistant from its boundary [27]. Skeletonization can be primarily achieved with two methods: incrementally thinning the region by morphological erosion while maintaining endpoints and connectivity (the so-called "topology-preserving thinning"), or by computing the medial axis of the region and adopting the medial axis transform introduced by Blum [28].

In this study, as illustrated in figure 2, the medial axis-based approach to skeletonization was employed. The medial axis of the binary image, along with the distance transform which quantifies the distance from each pixel to the nearest background pixel, was computed during skeletonization. The crack length is implicitly represented by the total number of pixels in the skeletonized image, with each pixel corresponding to a segment of the crack. The crack width was determined using the distance transform, which provides the minimum distance from a skeleton pixel to the nearest background pixel. The crack width is calculated as twice this distance, effectively capturing the physical width of the crack. In this study, the scaling factor in the used test image is 883,642 nm/Px. The DPI (Dots Per Inch) for the image is 300×300.

After extracting the geometry of the crack, if its width is larger than 3mm it can be deemed large enough to allow airflow throughout its length (ASHRAE [29]).

Airflow through cracks in buildings envelopes

Airflow through cracks

The transport of fluid through a crack is governed by the pressure differential imposed across the structural boundary of the building. The volumetric discharge rate is intrinsically dependent on the manner in which pressure forces are distributed and dissipated along the pressure gradient. Pressure dissipation within the crack occurs via three principal mechanisms: viscous resistance, inertial effects, and fluid expansion [30]. An idealized representation of the straight-through crack geometry is provided in figure 3.

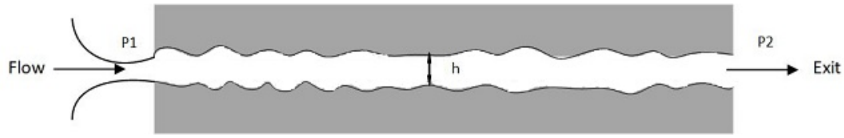

Figure 3. Representation of the airflow through straight-through crack

Within the scope of this work, the influence of tortuosity is deliberately excluded to simplify the theoretical framework. According to the analysis of surface cracks detected in structural components under tensile or bending loads, the distribution of crack opening displacement per unit nominal stain along a surface crack line appears to be proportional to the crack depth distribution. The distribution of the crack depth $\delta(x)$ can be approximated by multiplying an amplifier α to the distribution of $\frac{\delta(x)}{\varepsilon_n}$ of a surface crack initiated in structural member subjected to a bending load, with ε_n the nominal strain. Developing a mathematical model to generate crack morphology that incorporates the tortuous path of the cracks into its geometric description, at gross level due to millimeter-size aggregates, as well as at refined level due to micro-size grains within the cement paste, enables direct numerical discretization of the Navier-Stokes equations for fluid flow studies through the crack path. Such a computational model containing all geometric features to the smallest scale that can affect fluid flow is expected to represent all possible ranges of flow field through cracks, to handle wide ranges of pressure gradients and crack widths of practical significance [31].

The relationship between crack width (w) and crack depth (d), in drying-induced cracks on timber surfaces, often follows an approximately linear or lightly exponential trend, particularly in early stages of crack formation. Crack depth in timber structures can range from 3 to 10 times the crack width [32]. In brick masonry, crack width is a critical factor affecting durability, especially with regard to water intrusion. The depth of cracks with widths as small as 0.1 mm often correlates with their width [33]. In concrete structures, the correlation between crack width, depth, and length is influenced by factors such as loading conditions and reinforcement [34].

Moreover, the airflow through the crack is postulated to exhibit laminar behavior, thereby neglecting any potential contributions from turbulence. Accordingly, the airflow is modeled based on the canonical equation for laminar flow through infinitely parallel plates, derived from the quadratic velocity distribution [35]:

$$\frac{Q}{L} = \frac{d^3 \Delta P_f}{12\mu z}\,. \tag{6}$$

In Eq. (6), ΔP_f denotes the pressure drop attributable to skin friction along the z-dimension in the flow direction, d corresponds to the thickness of the gap, L represents the breadth of the plates, and μ refers to the dynamic viscosity of the fluid, quantified as 1.81×10^{-5}. All the relevant parameters are delineated in the accompanying figure.

Air infiltration

Infiltration airflow is induced by a pressure gradient across the building envelope, arising from three primary components: wind pressure, stack pressure, and the influence of any active ventilation systems, which collectively contribute to the overall driving pressure gradient [36]. Stack pressure is intrinsically dependent on building height and the differential between indoor and outdoor ambient air temperatures, whereas wind pressure is primarily influenced by factors such as wind velocity, direction, local terrain, topography, and the geometric characteristics of the building. The total pressure drop across the building envelope is written as in Eq. (7) [37]:

$$\Delta P_{\text{total}} = \Delta P_{\text{stack}} + \Delta P_{\text{wind}} + \Delta P_{\text{ventilation}} \,. \tag{7}$$

In this study, to establish an initial framework, the effects of wind and ventilation are neglected, focusing solely on the influence of stack pressure. The origin of the stack effect lies in the temperature gradient across the building envelope. According to the ideal gas law, air density (ρ) is inversely proportional to the temperature (T), as shown in Eq. (8). This temperature disparity between the interior and exterior of a building generates differences in air density [5, 37],

$$\rho = \frac{P}{RT} \,, \tag{8}$$

where ρ denotes air density (kg/m^3), P is air pressure (Pa), R represents the specific gas constant, and T is the air temperature (K). Consequently, variations in air density across the building envelope lead to buoyancy-driven differences in air pressure. This results in a vertical pressure gradient along the height of the building, referred to as the *stack effect*, which partially governs the infiltration airflow. The stack pressure gradient is height-dependent and can be expressed by Equation (9) [5],

$$\Delta P = \rho g h \,, \tag{9}$$

where g represents the gravitational acceleration constant (m/s^2), and h is the height of the air column. The neutral pressure level (NPL), denoted as y_{NPL}, is the height at which the internal pressure equals the external pressure, as illustrated in figure 3.

The stack pressure can be further quantified by using Equations (10-12), which assume well-mixed air on both sides of the building envelope [37],

$$\Delta P_{\text{stack}} = (\rho_{\text{out}} - \rho_{\text{in}})\, g y \,, \tag{10}$$

$$\Delta P_{\text{stack}} = -g \Delta h \left(\frac{\rho_{\text{out}}}{R_0 T_0} - \frac{\rho_{\text{out}}}{R_i T_i} \right) \,, \tag{11}$$

$$\Delta P_{\text{stack}} = \rho_{\text{out}} g \Delta h \left(\frac{T_i - T_0}{T_i} \right) \,, \tag{12}$$

where ρ_{in} and ρ_{out} [kg/m^3] represent the densities of indoor and outdoor air, respectively; Δh [m] denotes the vertical distance from the neutral pressure level (NPL), expressed as $\Delta h = h - \text{NPL}$; h [m] is the height of the crack zone above the base; and g [m/s^2] is the gravitational acceleration constant. ρ_{in} and ρ_{out} are determined according to Eq. (8).

Analysis and discussion

Application Example

In this work, a 4 story office building located in Tallinn, Estonia, is used as a case study to demonstrate the applicability of the proposed framework. The crack images from the dataset, captured from the wall's surface, are scaled proportionally to real-world dimensions, thereby enabling the framework to translate crack width and length into millimeters. Subsequently, employing the initial phase of the framework outlined in Figure 1, the images are analyzed to ascertain the presence or absence of cracks. Figures 4 and 5 illustrate the input images alongside the corresponding output results generated by the crack detection module of the framework.

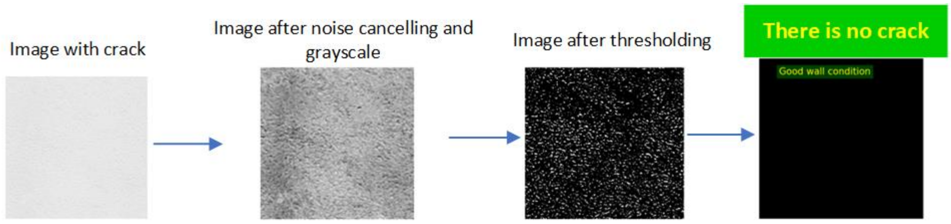

Figure 4. Crack detection for a surface without crack

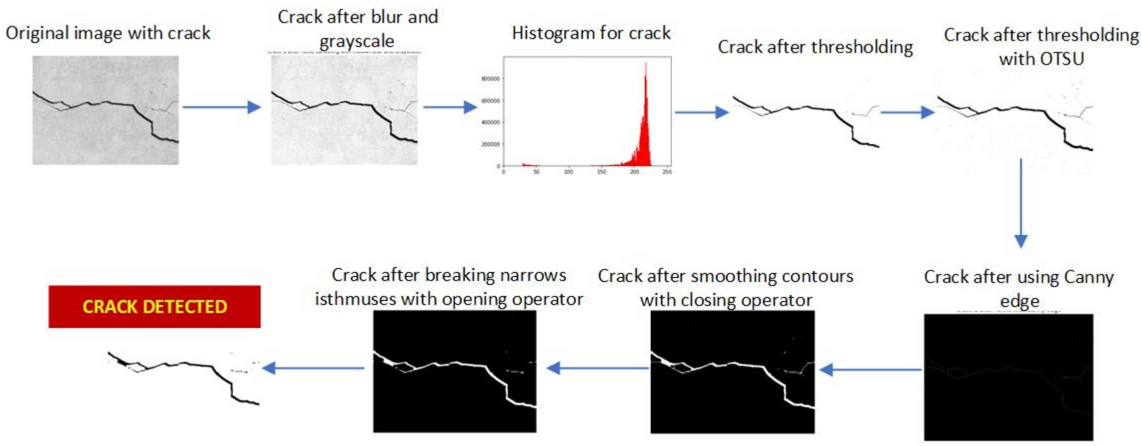

Figure 5. Crack detection for a surface with crack

According to figure 4, it is significant to see that after noise cancellation and thresholding, no crack is detected from the image.

Table 1 provides a detailed comparison of the crack morphology obtained through the second stage of the framework,in Figure 5, against the actual measured dimensions of the crack. The analysis demonstrates that the mean crack width is 4.35 mm, which notably exceeds the critical threshold of 3 mm, indicating its potential significance as a contributor to airflow and energy dissipation. As shown in the table, the differences between real measurements and computer vision (CV)-based measurements for maximum width, minimum width, mean width, and length are 1.3%, 1.05%, 16.5%, and 1.17%, respectively, with the CV measurements consistently slightly exceeding the real values. Despite these discrepancies, the measurements achieved through the framework exhibit a high degree of accuracy, validating its potential for practical applications in automated crack morphology assessment.

In the final stage of the proposed framework, the identified crack, detected via the imported image, is analyzed at a height of 6.5 meters above the ground level, with the neutral pressure plane (NPP) situated 4.5 meters above the same reference point. The wall under consideration has a depth of 0.35 meters. By using Equations (6) to (12) as

Table 1. Comparison of real and computer vision measurements of crack width and length.

Crack Type	max w. [mm]	min w. [mm]	mean w. [mm]	length [mm]
Real measurement	6.95	0.006	3.478	59.0
CV measurement	7.035	0.00667	4.1558	59.7

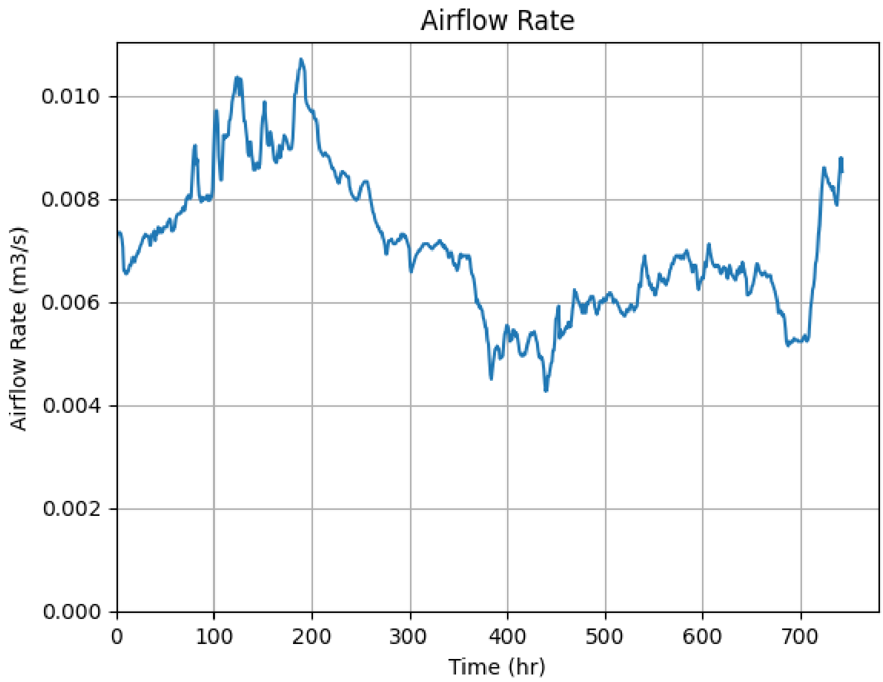

Figure 6. Airflow rate through the crack in December 2021

input to a Python script, hourly outdoor dry bulb air temperature data for December 2021 in Tallinn were incorporated into the computational model. This facilitated the determination of the stack-induced pressure drop within the localized region of the building envelope where the crack is present. Subsequently, the hourly fluctuation of airflow through the identified crack was estimated using Equation (6).

The results, which illustrate the temporal variation in airflow rates during December 2021, are presented in figure 5. This visualization underscores the dynamic nature of infiltration as driven by stack effects, highlighting the influence of temperature variations on the pressure gradient and consequent airflow through the crack. These findings offer critical insights into the relationship between crack morphology and its contribution to air leakage, particularly under varying environmental conditions. According to figure 6, considering stack effect on airflow through the issued crack is feasible.

Conclusions

Airflow through cracks and splits represents a significant pathway for energy dissipation in buildings, highlighting the critical need for automated methodologies to accurately measure crack areas. In this study we have proposed a novel computer vision-based framework for the detection and detailed estimation of the geometry of straight-through cracks in building envelopes. Coupling this artificial intelligence method with governing physical equations, it was shown that an integration between fluid mechanics of airflow and automated geometric quantification of cracks using image processing can estimate and even predict airflow through cracks.

It was found that the differences between real measurements and CV-based measurements are quite negligible, of the order 1% for maximum width, minimum width, and length. Only for mean width this difference is more substantial and amounts to 17%. In any case, these are encouraging results for this first stage of investigation.

The proposed framework offers a novel approach to replace manual measurements with an automated process for detecting and quantifying cracks across all walls and rooms within a building. By categorizing detected cracks and estimating potential airflow through them, this method provides a systematic tool for energy analysis.

The proposed method features an effective vision-based method for wall crack detection that has practical value towards many applications. The framework has been evaluated on various images, and can successfully extract visible cracks from the background of images captured by an inspection robot. The obtained results are consistent with different data sources, with a distinct number as well as the visibility level of the detected crack. The threshold for image binarization is employed from a non-parametric peak detection algorithm. A quantifiable criterion for air tightness measurement is also established by estimating the total surface area of splits and cracks, as well as the potential airflow through them considering different scenarios that cause varying pressure differentials.

In the morphological analysis stage of this study, the cross-sectional area of the cracks is approximated as rectangular, enabling an efficient estimation of crack dimensions. This framework eliminates the reliance on manual measurements or thermal imaging devices by providing an automated calculation of crack areas and subsequent airflow estimation. Furthermore, with the integration of this framework into augmented or virtual reality environments, it is possible to generate detailed thermal maps. These maps can illustrate airflow distribution, highlighting the sections of cracks with the highest airflow rates based on the minimum and maximum detected cross-sectional areas. The automation and scalability of this formalism offer a transformative step toward enhanced building energy assessments, by enabling comprehensive crack analysis at both micro and macro scales, ultimately supporting more efficient energy saving strategies.

In conclusion, our proposed method could be considered as fully automatic, thus it could substantially enhance the ability to recognize airflow through the splits and cracks of a room within a robotic inspection process.

Several considerations are needed on different aspects anyway, since this is a first step in a novel methodology and several limitations do exist.

In this research, the cracks are assumed to be straight-through without tortuosity to simplify the analysis. Assuming straight cracks has a clear limitation on practical grounds, since straight-through cracks are not likely to occur in many real cases; in reality, cracks exhibit a more convoluted and irregular shape. The crack width is here considered as the mean of measured widths of the crack through the image, which is indeed affected by the largest 17% error. Future work is thus expected on exploring different crack path geometries, including L-shaped and multi-cornered configurations through integral methods, to recognize the precise amount of the area of the crack on the wall and the way of the propagation, including prediction of the variation in airflow in different time frames. In addition, the use of physically precise calculations is expected to estimate the probability of a crack propagating through the full thickness of the envelope.

More advanced segmentation methods, e.g., segment anything, could also be used. Once the model has been thus enhanced, thorough fluid dynamics experiments should also be performed in various conditions, for complete testing with accurate data sources. Finally, the fluid dynamics equations for the physics module can be refined via computational fluid dynamics (CFD) modeling, which will enhance accuracy. All these observations pose research questions and set a well-defined strategy for future work.

References

[1] Energiatehokkuus Ympäristöministeriö. Rakennuksen energiankulutuksen ja lämmitystehontarpeen laskenta. *Ministry of the Environment, Energy efficiency, Calculation of building energy consumption and heating power demand), Regulation, Helsinki, Finland*, 2018.

[2] Juha Jokisalo, Jarek Kurnitski, Minna Korpi, Targo Kalamees, and Juha Vinha. Building leakage, infiltration, and energy performance analyses for finnish detached houses. *Building and Environment*, 44(2):377–387, 2009.

[3] Mark Y Ackerman, Doug Dale, David Wilson, and Bailey Ryan. Infiltration heat recovery, part 1: field studies in an instrumented test building. *ASHRAE transactions*, 112(2):597–609, 2006.

[4] Ake K Blomsterberg and David T Harrje. Approaches to evaluation of air infiltration energy losses in buildings. *ASHRAE Transactions*, 85(1):797–815, 1979.

[5] Chadi Younes, Caesar Abi Shdid, and Girma Bitsuamlak. Air infiltration through building envelopes: A review. *Journal of Building physics*, 35(3):267–302, 2012.

[6] Andrea Ferrantelli, Camilla Vornanen-Winqvist, Milla Mattila, Heidi Salonen, and Jarek Kurnitski. Positive pressure effect on moisture performance in a school building. *Journal of Building Physics*, 43(2):121–142, 2019.

[7] PT McGrath, E Lai, and M Roche. Air infiltration through cracks in suspended timber floors. *Building Services Engineering Research and Technology*, 20(2):45–50, 1999.

[8] Lisa C Ng, Stephen Zimmerman, Jeremy Good, Brian Toll, Steven J Emmerich, and Andrew K Persily. Estimating real-time infiltration for use in residential ventilation control. *Indoor and Built Environment*, 29(4):508–526, 2020.

[9] PH Baker, S Sharples, and IC Ward. Air flow through cracks. *Building and Environment*, 22(4):293–304, 1987.

[10] DW Etheridge. Crack flow equations and scale effect. *building and environment*, 12(3):181–189, 1977.

[11] Haifeng Li, Dezhen Song, Yu Liu, and Binbin Li. Automatic pavement crack detection by multi-scale image fusion. *IEEE Transactions on Intelligent Transportation Systems*, 20(6):2025–2036, 2018.

[12] Yu-Fei Liu, Soojin Cho, BF Spencer Jr, and Jian-Sheng Fan. Concrete crack assessment using digital image processing and 3d scene reconstruction. *Journal of Computing in Civil Engineering*, 30(1):04014124, 2016.

[13] Nhat-Duc Hoang, Thanh-Canh Huynh, Xuan-Linh Tran, and Van-Duc Tran. A novel approach for detection of pavement crack and sealed crack using image processing and salp swarm algorithm optimized machine learning. *Advances in Civil Engineering*, 2022(1):9193511, 2022.

[14] Kesari Verma, Bikesh Kumar Singh, and AS Thoke. An enhancement in adaptive median filter for edge preservation. *Procedia Computer Science*, 48:29–36, 2015.

[15] Chul Min Yeum and Shirley J Dyke. Vision-based automated crack detection for bridge inspection. *Computer-Aided Civil and Infrastructure Engineering*, 30(10):759–770, 2015.

[16] Rafael C. Gonzalez and Richard E. Woods. *Digital Image Processing.* Pearson, Harlow, UK, 4th edition, 2018.

[17] Richard Szeliski. *Computer vision: algorithms and applications.* Springer Nature, 2022.

[18] G Jyothi, C Sushma, and DSS Veeresh. Luminance based conversion of gray scale image to rgb image. *Int. J. Comput. Sci. Inf. Technol. Res*, 3(3):279–283, 2015.

[19] Arun Mohan and Sumathi Poobal. Crack detection using image processing: A critical review and analysis. *alexandria engineering journal*, 57(2):787–798, 2018.

[20] Hyunjun Kim, Eunjong Ahn, Soojin Cho, Myoungsu Shin, and Sung-Han Sim. Comparative analysis of image binarization methods for crack identification in concrete structures. *Cement and Concrete Research*, 99:53–61, 2017.

[21] Qijun Luo, Baozhen Ge, and Qingguo Tian. A fast adaptive crack detection algorithm based on a double-edge extraction operator of fsm. *Construction and Building Materials*, 204:244–254, 2019.

[22] Nhat-Duc Hoang and Quoc-Lam Nguyen. Metaheuristic optimized edge detection for recognition of concrete wall cracks: a comparative study on the performances of roberts, prewitt, canny, and sobel algorithms. *Advances in Civil Engineering*, 2018(1):7163580, 2018.

[23] Gaochao Wang, W Tse Peter, and Maodan Yuan. Automatic internal crack detection from a sequence of infrared images with a triple-threshold canny edge detector. *Measurement Science and Technology*, 29(2):025403, 2018.

[24] MM Sarker, TA Ali, A Abdelfatah, S Yehia, and A Elaksher. A cost-effective method for crack detection and measurement on concrete surface. *The International Archives of the Photogrammetry, Remote Sensing and Spatial Information Sciences*, 42:237–241, 2017.

[25] Edward R Dougherty and Roberto A Lotufo. *Hands-on morphological image processing*, volume 59. SPIE press, 2003.

[26] Pierre Soille et al. *Morphological image analysis: principles and applications*, volume 2. Springer, 1999.

[27] Aiguo Ouyang, Chagen Luo, and Chao Zhou. Surface distresses detection of pavement based on digital image processing. In *Computer and Computing Technologies in Agriculture IV: 4th IFIP TC 12 Conference, CCTA 2010, Nanchang, China, October 22-25, 2010, Selected Papers, Part IV 4*, pages 368–375. Springer, 2011.

[28] Harry Blum. A transformation for extracting new descriptions of shape. *Models for the perception of speech and visual form*, pages 362–380, 1967.

[29] R.R. Johnson and American Society of Heating. *Fundamentals of HVAC Systems: ASHRAE Learning Institute*. American Society of Heating, Refrigerating & Air-Conditioning Engineers, Incorporated, 2003.

[30] SBM Beck, NM Bagshaw, and JR Yates. Explicit equations for leak rates through narrow cracks. *International journal of pressure vessels and piping*, 82(7):565–570, 2005.

[31] Jingxia Yue, Yukio Fujimoto, and Taufiq A Setyanto. Estimation of surface crack depth based on measurement of crack opening deformation. In *ISOPE International Ocean and Polar Engineering Conference*, pages ISOPE–I. ISOPE, 2005.

[32] Florian Brandstätter, Maximilian Autengruber, Markus Lukacevic, and Josef Füssl. Prediction of moisture-induced cracks in wooden cross sections using finite element simulations. *Wood Science and Technology*, 57(3):671–701, 2023.

[33] K Koocheki and S Pietruszczak. Mesoscale analysis of fracture process in brick masonry structures. *Mathematics and Mechanics of Solids*, 30(1):73–92, 2025.

[34] Yue Li, Juhui Zhang, Zhongguo Guan, and Youliang Chen. Experimental study on the correlation between crack width and crack depth of rc beams. *Materials*, 14(20):5950, 2021.

[35] Chung Fang. *An introduction to fluid mechanics*, volume 935. Springer, 2019.

[36] Karl Grau Sørensen and Carsten Rode. Implementation of models for building envelope air flow fields in a whole building hygrothermal simulation tool. In *Proceedings of the 4th international building physics conference: Energy efficiency and new approaches, 15-18 June 2009, Istanbul*. Istanbul Technical University, 2009.

[37] Jan F Kreider, Peter S Curtiss, and Ari Rabl. *Heating and cooling of buildings: design for efficiency*. CRC Press, 2009.

Maliheh Jahanbakhsh and Andrea Ferrantelli
Department of Civil Engineering, Aalto University
00076 Aalto, Finland
maliheh.jahanbakhsh@aalto.fi, andrea.1.ferrantelli@aalto.fi

Andrea Ferrantelli
Department of Energy and Mechanical Engineering, Aalto University
00076 Aalto, Finland
Department of Civil Engineering and Architecture, Tallinn University of Technology
Ehitajate tee 5, 19086 Tallinn, Estonia
andrea.ferrantelli@taltech.ee